Accepted Manuscript

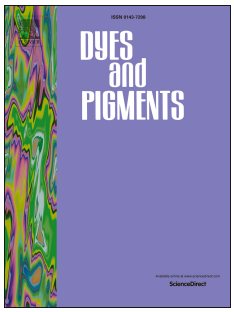

Two-photon excited organic nanoparticles for chemo-photodynamic therapy

Tao Zhang, Li Fu, Xiaohua Zheng, Ming Liu, Qing Pei, Xue Wang, Shi Liu

PII: S0143-7208(19)30240-2

DOI: https://doi.org/10.1016/j.dyepig.2019.04.038

Reference: DYPI 7493

To appear in: *Dyes and Pigments*

Received Date: 29 January 2019

Revised Date: 9 April 2019

Accepted Date: 15 April 2019

Please cite this article as: Zhang T, Fu L, Zheng X, Liu M, Pei Q, Wang X, Liu S, Two-photon excited organic nanoparticles for chemo-photodynamic therapy, *Dyes and Pigments* (2019), doi: https://doi.org/10.1016/j.dyepig.2019.04.038.

Two-Photon Excited Organic Nanoparticles for Chemo-Photodynamic Therapy

Tao Zhang [a], Li Fu [c], Xiaohua Zheng [b], Ming Liu [b], Qing Pei [b], Xue Wang [a*], Shi Liu [b*]

[a] China-Japan Union Hospital of Jilin University, 126 Xiantai Street, Changchun, Jilin 130033, P. R. China. E-mail: wangxue2263@163.com

[b] State Key Laboratory of Polymer Physics and Chemistry, Changchun Institute of Applied Chemistry, Chinese Academy of Sciences, Changchun 130022 (China). E-mail: liushi@ciac.ac.cn

[c] Department of Implantology, Stomatological Hospital, Jilin University, Changchun 130021, P.R.China

Keywords: paclitaxel; two-photon; photodynamic therapy; chemotherapy.

Abstract

Drug molecules assembling nanomedicines possess several advantages, including precise molecular structure, various combinations of theraputic agents and high content of drugs. In this work, paclitaxel dimer and two-photo photosensitizer were devised and synthesized, which could coassemble into nanoparticles (Co-NPs) in aqueous medium through nanopreicipitation method. As-synthesized Co-NPs possess the uniform size of about 80 nm and great stability in physiological condition, and could produce the singlet oxygen upon near-infrared light irradiation. The Co-NPs indicate enhanced cellular uptake and endosomal escape upon irradiation, which result in the synergistic enhancement of cytotoxicity towards cancer cells and growth inhibition of human cervical cancer tumors. We believed this combination therapy based on organic nanoparticles represent a new and important development in the cancer therapy.

Introduction

It is highly desired to develop efficient cancer therapies due to the complicated and heterogeneous solid tumor.[1, 2] Traditional single tumor treatments, including chemotherapy, radiotherapy and phototherapy, usually are hard to completely inhibit the tumor growth and recurrence.[3, 4] Combination of different therapy in one system is valuable and versatile for enhancing the therapeutic index and response.[5-15] Merging two and more therapies could be realized by encapsulating or conjugating therapeutic agents with polymer or other nanoparticles.[16, 17] Although great advance has been made in nanoformulation of antitumor drugs, the drug loading and loading efficiency is suboptimal. A large amount of drug carrier was

used for stabilizing the formulations, which result in the potential long term toxicity and the difficulties in enlarged production. Design of optimized drug carriers is imperative to improve the therapeutic outcomes and minimize undesirable side effects.[18]

Recently, the self-assembly of drug molecules provide a straightforward way for preparing nanoformulations of drugs.[19] Except of amphiphilic drug molecules,[20-22] some hydrophobic molecules could also assemble into nanoscale aggregates in aqueous medium through different mechanism, including disulfide-induced assembly,[23, 24] symmetrical dimer assembly[25-27] and conjugated molecules assembly. In our previous work, a number of paclitaxel (PTX) dimers was synthesized and could form the nanomedicines in the absence of surfactants or adjuvants.[28-30] Although the PTX dimers formed nanomedicines possess effective cellular uptake and cytotoxicity, and significant antitumor efficacy, the suboptimal tumor treatment could be improved through the combination therapy.

Chemotherapy drugs and photosensitizers were widely combined for overcoming drug resistance and enhancing the therapeutic response.[31, 32] As well as we know, the combination chemo and phototherapy in one organic nanoparticle isn't reported yet. We hypothesized the assembling PTX dimers and photosensitizers in one formulation could produce synergistic effect for tumor treatment. In order to increase the treatment depth, the photosensitizer possessed big absorption wavelength is indispensible for efficient antitumor efficacy.[29, 33-36] Herein, the two-photo excited photosensitizer (2PE-PS) is employed for the study in vitro and in vivo.[37-40] In this work, the PTX dimer with disulfide bond as linker (PTX-s-s-PTX) and 2PE-PS was used to construct a nanoprodrug in the absence of surfactants (Fig 1A), and their morphologies, photophysical properties, cellular uptake and cytotoxicity, and tumor inhibition was investigated in detail (Fig 1B).

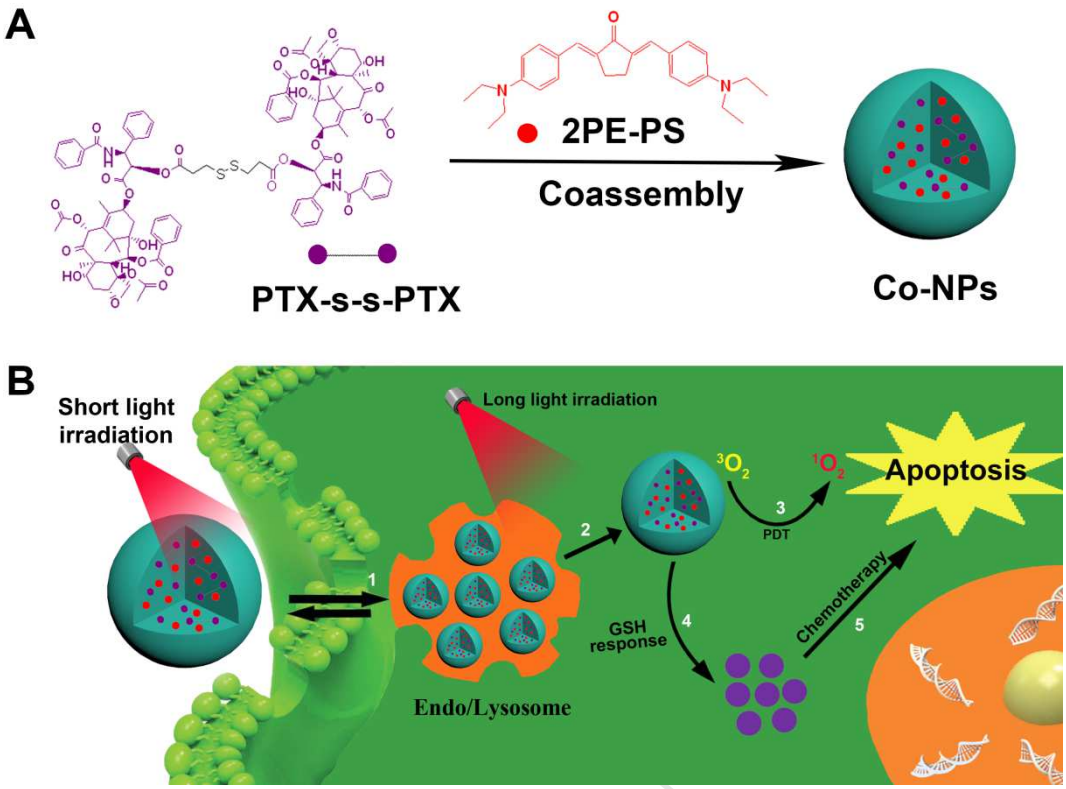

Fig 1. (A) Formation of Co-NPs. (B) Schematic of the synergistic chemotherapy and PDT. (1) Enhanced cell uptake by a short light irradiation for PCI effect. (2) Enhanced escape of Co-NPs from lysosome to the cytosol based on photochemical rupture of lysosome membranes. (3) Anticancer efficacy from photodynamic therapy. (4) Conversion of the PTX-SS prodrug into free PTX by GSH trigger. (5) Free PTX diffused to the cytosol for chemotherapy and induced cell death.

Experimental sections

Materials

1, 3-dicyclohexylcarbodiimide (DCC), 4-dimethylaminopyridine (DMAP) and paclitaxel were purchased from Sigma-Aldrich (St. Louis, MO, U.S.A.). 3,3-dithiodipropionic acid，sodium hydroxide and cyclopentanone were purchased from Shanghai Sun Chemical Technology Co., Ltd.. MTT and Lyso-Tracker Red were purchased from Beyotime Biotechnology Co., Ltd. (China). Live-Dead Cell Staining Kit was purchased from KeyGEN BioTECH Co., Ltd.. All of the other chemical substances were prepared commercially and were used without further purification, unless otherwise noted. All the solvents were purified according to the standard methods whenever needed.

Instruments

^{1}H NMR spectra were tested on a Bruker NMR-400 DRX spectrometer at room temperature. The mass spectra (MS) of all the samples were recorded by the German company Bruker autoflex III smartbeam MALDI-TOF/TOF mass spectrometer with a smart beam laser with a wavelength at 355 nm. UV-vis absorption spectra were recorded with a Shimadzu UV-2450 PC UV/Vis spectrophotometer. The fluorescence intensity tests were obtained using PerkinElmer LS-55 Spectrofluorophotometer. Zeta potential and size distribution of the nanoparticles were characterized by Malvern Zeta-sizer Nano for dynamic light scattering (DLS). The morphology of all the nanoparticles was measured by transmission electron microscopy (TEM), characterized by a JEOL JEM-1011 electron microscope operating at an acceleration voltage of 100 kV. Confocal laser scanning microscopy (CLSM) images were taken by using a Zeiss LSM 700 (Zurich, Switzerland).

Synthesis of PTX-s-s-PTX

PTX-s-s-PTX was synthesized by the method described in the previous literature.

Synthesis of 2, 5-Bis(4-(diethylamino)benzylidene) cyclopentanone (2PE-PS)

2,5-Bis(4-(diethylamino)benzylidene)cyclopentanone was synthesized according to the previous literature. Briefly, 0.2 g of sodium hydroxide (5 mmol) was added to a stirred solution of 1.68 g of cyclopentanone (20 mmol) and 4-diethylaminobenzaldehyde (7.08 g, 40 mmol) in 50 mL of ethanol, and the reaction mixture was refluxed for 12 h. After cooling to room temperature, the precipitate was filtered out and washed with water. The crude product was recrystallized using ethanol to give 2PE-PS (93%). ^{1}H NMR (400 MHz $CDCl_3$): d (ppm) 1.20 (t, 12 H, J = 7.08 Hz), 3.06 (s, 4 H), 3.42 (q, 8 H, J = 7.08 Hz), 6.69 (d, 4 H, J = 8.92 Hz), 7.50–7.52 (m, 6 H).30 MALDI-TOF-MS: m/z Calcd for $C_{27}H_{35}N_2O$ $[M + H]^+$ 403.27439; found 403.3.

Nanoparticles preparation

A solution of PTX-SS (1 mg) and 2PE-PS (1 mg) in 4 mL tetrahydrofuran was added dropwise into the 10 mL of deionized water under a constant stirring, and NPs were formed after evaporation of 4 mL tetrahydrofuran and dialysis in water for 2 days. Different molar ratios of PTX-SS and 2PE-PS could form the corresponding PTX/2PE-PS_0, PTX/2PE-PS_2, PTX/2PE-PS_5 and PTX/2PE-PS_{10} NPs by the same precipitation method.

Singlet oxygen detection, photostability and ROS stability of Co-NPs

To evaluate the reactive oxygen species generation ability of 2PE-PS, a chemical method by using DPBF was employed with UV-vis spectroscopy.[41] 2PE-PS dissolved in 3 mL of DMF were blended with DPBF (15 μg/mL) and then irradiated

with an 808 nm laser at an intensity of 0.1 W/cm^2. The absorption intensity of the DPBF at the maximum wavelength of 414 nm was detected every 1 min. DPBF solution alone was irradiated as control. As for the photostability, the Co-NPs containing 2PE-PS was irradiated by an 808 nm laser resource at an intensity of 1 W/cm^2 for 30 min. The absorption spectrum of 2PE-PS was recorded every 5 min. In order to detect the ROS stability of PTX-SS, 1 mg PTX-SS and 1 mg 2PE-PS was dissolved in DMSO, the ^{1}H NMR spectrum was detected before and after irradiation with the 808 nm laser for 20 min.

Intracellular ROS detection

Confocal laser scanning microscopy (CLSM) observation method was employed to detect the ROS generation in cells. Firstly, HeLa cells were incubated with Co-NPs for 4 h, and then, the culture medium was washed four times. Then, the DMEM solution containing DCFH-DA (10×10^{-6} M) was added to the six well plates and further incubated for 35 min. An 808 nm light irradiation was used subsequently (1 W/cm^2 for 5 min). The outcomes were observed with CLSM as soon as possible (excitation wavelength, 488 nm; emission band-pass, 500−550 nm)

Intracellular uptake studies, lysosome colocalization and lysosome permeability measurements by AO staining

To verify the cellular endocytosis, HeLa cells were seeded in 6-well plates at about 200,000 cells per well in 2 mL culture medium (Dulbecco Modified Eagle Medium containing 10% fetal bovine serum), supplemented with 100 U/mL penicillin and 100 U/mL streptomycin, and incubated at 37 ℃ in 5 % CO_2 atmosphere for 20 h. Then the cells were treated with 2PE-PS and incubated at 37 ℃ for another 0.5, 2, 4, 6 h. The different well plates were washed three times with PBS and tested with CLSM method and quantified by flow cytometry analysis. The cells were incubated at 4 ^{o}C for 0.5, 2 h at the same condition to study the effect of temperature on the uptake of Co-NPs by cells.

In order to track the Co-NPs in cells, lysosome colocalization was conducted. Briefly, the lysosomal compartments of the cultured HeLa cells were stained with the probe of Lyso-Tracker red DND-99. One group was irradiated by the 808 nm laser. Thereafter, the cells were fixed with 4% formaldehyde for 10 min at room temperature, and the cell nuclei were stained with 4, 6-diamidino-2-phenylindole (DAPI, excited by 405 nm). CLSM images of cells were taken by using a Zeiss LSM 700 (Zurich, Switzerland). AO (Acridine Orange) staining method was used to determine the changes in lysosomal membrane permeability. HeLa cells were plated in a 6-well plate at a concentration of 300,000 cells per well. After incubation for 24 h, the cells were incubated with Co-NPs for 4 h and irradiated 5 min with an 808 nm laser, then AO containing PBS was added to each well (at a concentration of 2.5 μg/ml). After 30 min of incubation with AO, cells were washed three times with PBS and examined with a fluorescence microscope (Nikon Eclipse TE2000-U). The

excitation and emission wavelength of red fluorescence was 555 nm and 617 nm, and that of green fluorescence was 490 nm and 528 nm. AO concentrated in lysosomes emits a red fluorescence, whereas AO in the cytosol emits a green fluorescence. A reduction in red fluorescence along with an increased intensity of green fluorescence indicates a relocation of AO from the lysosomes to the cytosol, following by the change of lysosome permeability.

In vitro cytotoxicities on HeLa and HepG2 cells

HeLa and HepG2 cells obtained at a logarithmic growth phase were seeded in 96-well plates at a density of 5×10^3 cells per well and incubated in culture medium for 24 h. The media were then replaced by three different molar ratios of Co-NPs at various concentrations. The incubation was continued for 6 h. Then, the three groups were irradiated by a laser with a wavelength of 808 nm at 1 W/cm^2 for 15 min. After 48 h, the above culture medium was replaced by PBS and then 20 μL of MTT solution in PBS with the concentration of 5 mg/mL was added and the 96-well plates were incubated for another 4 h at 37 °C, followed by removal of the PBS containing MTT and addition of 150 μL of dimethyl sulfoxide (DMSO) to each well to dissolve the formazan crystals formed. Finally, the plates were shaken for 3 min, and the absorbance of formazan crystals dissolved was measured at 490 nm by a micro plate reader.

Calcein-AM/PI test

To visually demonstrate the anticancer efficacy of Co-NPs in chemotherapy and photodynamic therapy, the HeLa cells were stained with propidium iodide (PI) and calcein-AM (AM) to distinguish dead (red) and live (green) cells, respectively. The control and drug-treated cells were incubated in 96-well plates at 37 °C for 24 h in a humidified atmosphere containing 5% CO_2. Then, the cells were incubated with the drugs for 6 h, and then 2PE-PS and Co-NPs dishes of cells were irradiated for 15 min with an 808 nm laser at an intensity of 1 W/cm^2. Then, the cells were further incubated at 37 ^{o}C for another 48 h. After 48 h, the cells were stained with calcein-AM/PI for 35 min and washing with PBS, the samples of cells were imaged with a fluorescence microscope.

In vivo studies

Male nude mice were obtained and maintained under appropriate conditions. All the subsequent animal procedures have been approved and controlled by the local ethics committee and carried out according to the guidelines of Chinese law concerning the protection of animal life. To evaluate the antitumor activity, subcutaneous human cervical carcinoma HeLa tumor xenografts were utilized as animal modal. HeLa cells were subcutaneously inoculated into the rear backside of mice (4×10^6 cells in 0.1 mL PBS). The tumor-bearing male mice were randomly

divided into three groups (n=4): (1) blank control (PBS+Laser), (2) Co-NPs and (3) Co-NPs+Laser groups. Before treatment, three groups of mice were marked, weighed and measured, and then the tumor-bearing mice from Co-NPs and Co-NPs+Laser groups were intratumorly injected with Co-NPs at the dose of 1.9 mg kg^{-1} (drug weight/body weight), respectively. At designed time (every other day), body weight and tumor volume of mice were measured. At day 20, all the mice were sacrificed, and tumor was excised to intuitionally evaluate the tumor inhibition effect.

Results and discussion

Preparation and Characterization of Coassembly Nanoparticles (Co-NPs)

PTX-s-s-PTX conjugates (PTX-SS)[26] and 2PE-PS[32] were synthesized according to a method described previously. Their chemical structures were well confirmed by ^{1}H and ^{13}C NMR spectroscopy (Fig S1A-B and Fig S2A-B). The peaks at 1880 and 403.3 in the MALDI-TOF mass spectrum further validated the successful synthesis of the targeting molecules (Fig S1C and Fig S2C). The elution time of PTX-SS at 6.72 min obtained from high performance liquid chromatography (HPLC) method identified the purity. (Fig S1D) PTX-SS and 2PE-PS can form the nanoparticles (PTX-SS and 2PE-PS NPs) individually, and coassemble into nanoparticles (Co-NPs) in aqueous solution through a well-documented nano-precipitation method. Briefly, a solution of PTX-SS and 2PE-PS in tetrahydrofuran was added dropwise into the deionized water under regular stirring, and NPs were formed after evaporation of tetrahydrofuran and dialysis against water. Different molar ratios of PTX-SS and 2PE-PS in feed could form the corresponding PTX/2PE-PS_0, PTX/2PE-PS_2, PTX/2PE-PS_5 and PTX/2PE-PS_{10} NPs by the same precipitation method.

The morphology and size distribution of formed PTX-SS, 2PE-PS and Co-NPs NPs were characterized by transmission electron microscopy (TEM) and dynamic light scattering (DLS), respectively. As shown in Fig. 2A-C, the PTX-SS, 2PE-PS and Co-NPs NPs all possess a spherical morphology with a size of about 80 nm, while the corresponding DLS analysis shows that they have hydrodynamic diameters of 210 nm, 140 nm and 180 nm, respectively. The size, PDI and zeta potentials measured by DLS were listed in Table S1. The size and size distribution of three as-obtained NPs almost kept unchanged up to two weeks at room temperature, which indicated the resulting NPs hold good stability in water and fetal bovine serum (FBS) (Fig S3). The zeta potentials of PTX-SS, 2PE-PS, Co-NPs NPs are around -20, -17.3, -18.7 mV, respectively (Fig 2D). This negative surface charge can not only stabilize the as-prepared NPs by electrostatic repulsion but also reduce the serum protein adsorption. All these favorable properties are beneficial for their future biomedical applications.[42]

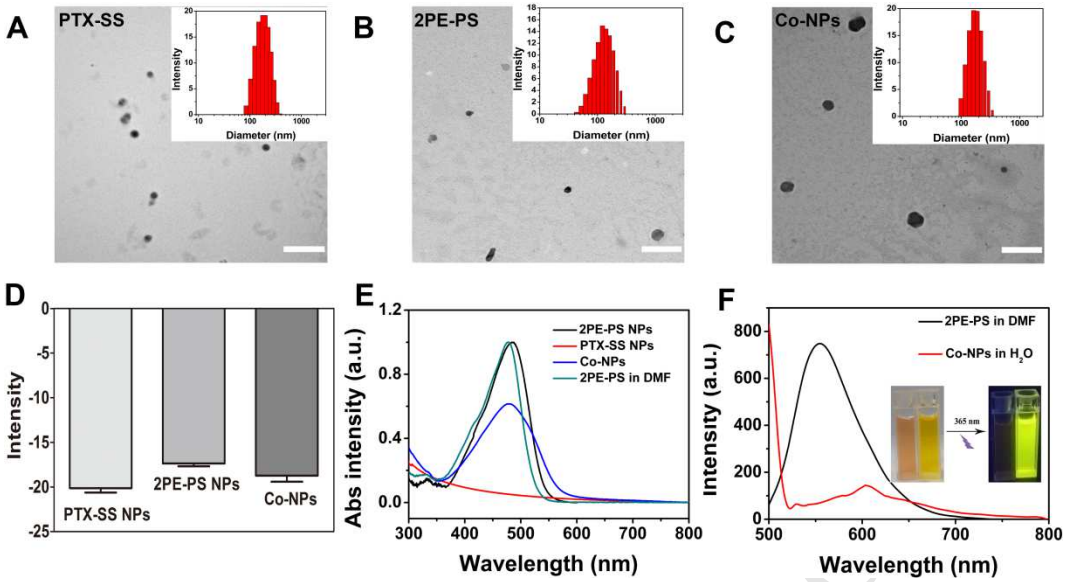

Fig 2. (A-C) TEM images and size distribution (DLS) of PTX-SS NPs, 2PE-PS NPs, Co-NPs. Scale bars: 200 nm. (D) Zeta potentials of PTX-SS NPs, 2PE-PS NPs, Co-NPs. (E) UV-vis absorption of 2PE-PS NPs, PTX-SS NPs, Co-NPs in water and 2PE-PS in DMF. (F) Fluorescence spectra of Co-NPs in water and equal concentration of 2PE-PS in DMF.

Photochemical Properties

We also recorded photophysical properties of 2PE-PS molecules in dimethyl formamide (DMF) and the 2PE-PS, PTX-SS, Co-NPs NPs dispersed in water, respectively. As shown in Fig 2E, the maximum absorption of 2PE-PS in DMF is 477 nm, which appeared red shifted to 484 nm when forming the aggregated nanoparticles. The typical absorption of 2PE-PS could be observed in that of Co-NPs in aqueous solution. The absorption band of PTX-SS is below 300 nm, imposing no obvious effect on the absorption of Co-NPs. The 2PE-PS molecules in DMF display an obvious orange florescence excited at 480 nm. By contrast, Co-NPs exhibit negligible fluorescence due to aggregation-induced quenching (Fig 2F).

The photochemical ability of the 2PE-PS to generate reactive oxygen species upon irradiation of 808 nm laser was studied by using 1,3-diphenylisobenzofuran (DPBF) and 2′,7′-dichlorodihydrofluorescein diacetate (DCFH-DA) as the indicator,[43-45] and the absorbance of DPBF was monitored by UV−vis absorption spectra. As a control experiment, DPBF (15 μg/mL) was irradiated in DMF without 2PE-PS. As shown in Fig 3B, only a negligible decrease in the absorbance of DPBF was found upon light irradiation, which reveals that DPBF is stable upon 808 nm laser irradiation. In sharp contrast, irradiation of a solution of DPBF (15 μg/mL) in DMF (3 mL) with laser at an intensity of 0.1 W/cm^2 in the presence of 2PE-PS (5 μg) causes a steady generation of reactive oxygen species, as evidenced by the absorption peak of DPBF at 414 nm decreasing upon oxidative degradation by $^1O_2$ (Fig 3A). A time-dependent plot of the DPBF absorbance at 414 nm (Fig 3B) reveals that the DPBF is consumed

rapidly in the presence of 2PE-PS upon laser irradiation. As an important property of photosensitizers, photostability of Co-NPs is investigated. As shown in Fig S4A, the absorption of Co-NPs almost kept unchanged under irradiation of an 808 nm laser at 1 W/cm^2 for 30 min, indicating the favorable optical stability. Above results identified that the Co-NPs could efficiently generate ROS in vitro. Because the PTX-SS existed in the Co-NPs, it was necessary to test the stability of PTX-SS molecule in the presence of ROS. PTX-SS and 2PE-PS were dissolved in DMSO, and then irradiated with an 808 nm laser at 1 W/cm^2 for 20 min. As shown in Fig S4B, the NMR spectra showed no changes before and after irradiation, validating that PTX-SS would not be destroyed by ROS before it exerts the effect of subsequent anticancer therapy.

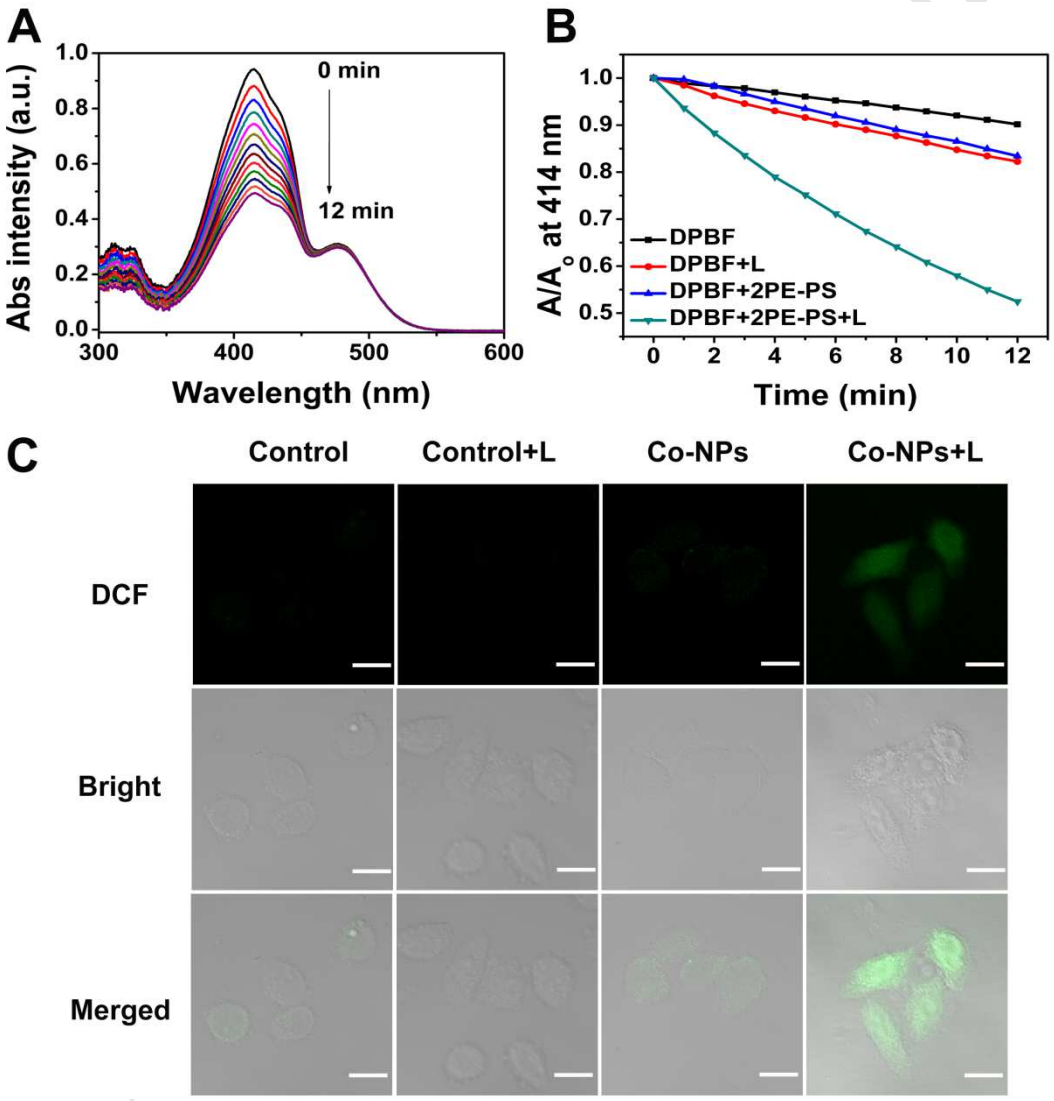

Fig 3. Singlet oxygen generation ability of as-prepared Co-NPs. (A) Time-dependent UV absorption spectra of DPBF at 414 nm with 2PE-PS in DMF after irradiation with an 808 nm laser from 0 to 12 min. (B) Comparison of the decay rate of DPBF with and without irradiation, treated with 2PE-PS along with or without irradiation. (C) The generation of intracellular ROS mediated by Co-NPs upon light irradiation of 0.1 W/cm^2 for 5 min indicated by the fluorescence of DCF about the blank control with

and without irradiation, pretreated with Co-NPs along with or without laser treatment. Scale bars, 20 μm.

Besides, intracellular ROS generation by Co-NPs in cervical cancer cells (HeLa cells) was further detected by using DCFH-DA as indicators under confocal laser scanning microscopy (CLSM). As shown in Fig 3C, almost no green fluorescence is observed in all control groups, because there is no adequate singlet oxygen in cells to oxidize nonfluorescent DCFH-DA into fluorescent dichlorofluorescein (DCF). By comparison, a bright green fluorescence appears in Co-NPs group under light irradiation due to the formation of singlet oxygen. Hence, such Co-NPs can be potentially applied as photosensitizers for photodynamic therapy.

Cell uptake properties

It is well known that effective cell internalization of drugs is vital to the efficacy of both PDT and chemotherapy. The cellular endocytosis of Co-NPs in HeLa cells was investigated by using CLSM and flow cytometry. The cell nuclei are stained with the dye of DAPI. CLSM images (Fig S5) and flow cytometry (Fig 4A, A1) show an enhanced intracellular distribution of Co-NPs in HeLa cells with the extension of incubation time from 0.5 h to 6 h. The uptake of Co-NPs increased obviously when the incubation temperature increased from 4 °C to 37 °C, indicating the ATP-mediated endocytosis (Fig. S5).

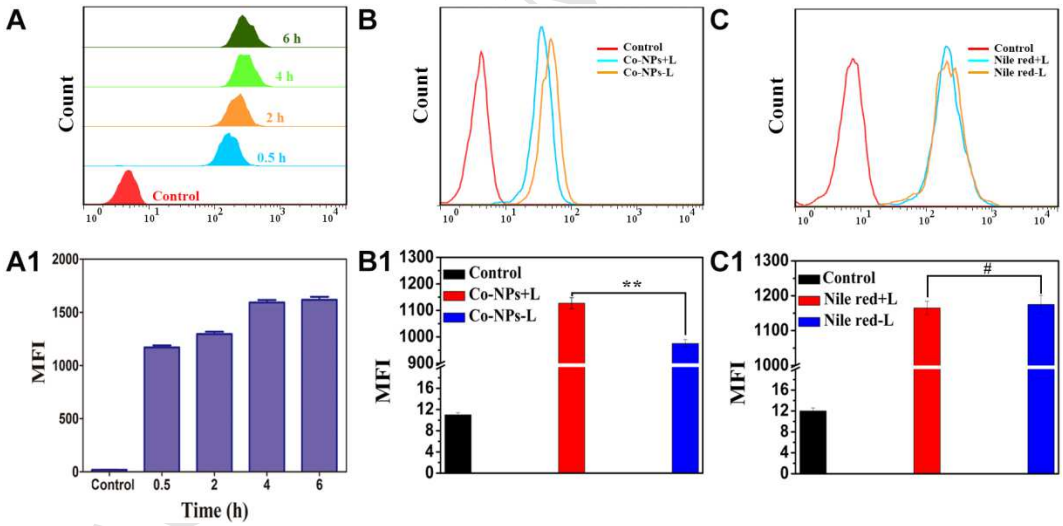

Fig 4. (A) Flow analysis and (A1) mean fluorescence intensity of different time of Co-NPs after uptaked by HeLa cells. (B–C) Flow cytometric analysis of HeLa cells pretreated with Co-NPs and NPs (PTX-SS+Nile red) with (+L) or without (−L) 3 min laser irradiation during internalization. Cells without any treatments were used as control. (B1–C1) Mean fluorescence intensity of HeLa cells treated with the two NPs. **$p < 0.01$, #$p > 0.05$.

Lysosome colocalization research was carried out by using the probe of Lyso-tracker Red. HeLa cells were incubated with Co-NPs for 2 h and then stained

with Lyso-tracker Red at 37 ^{o}C for 30 min.[46-50] As shown in Fig 5, Co-NPs nanoparticles mainly locate within the lysosome. Under the same condition, cells were incubated for 2 h and then irradiated with an 808 nm laser for 5 min. Compared to the non-irradiated control, the green fluorescence of Co-NPs and red fluorescence of Lyso-tracker Red decreased remarkably, which indicated that the laser irradiation facilitate the escape of Co-NPs from lysosome to cytoplasm (Fig 5).

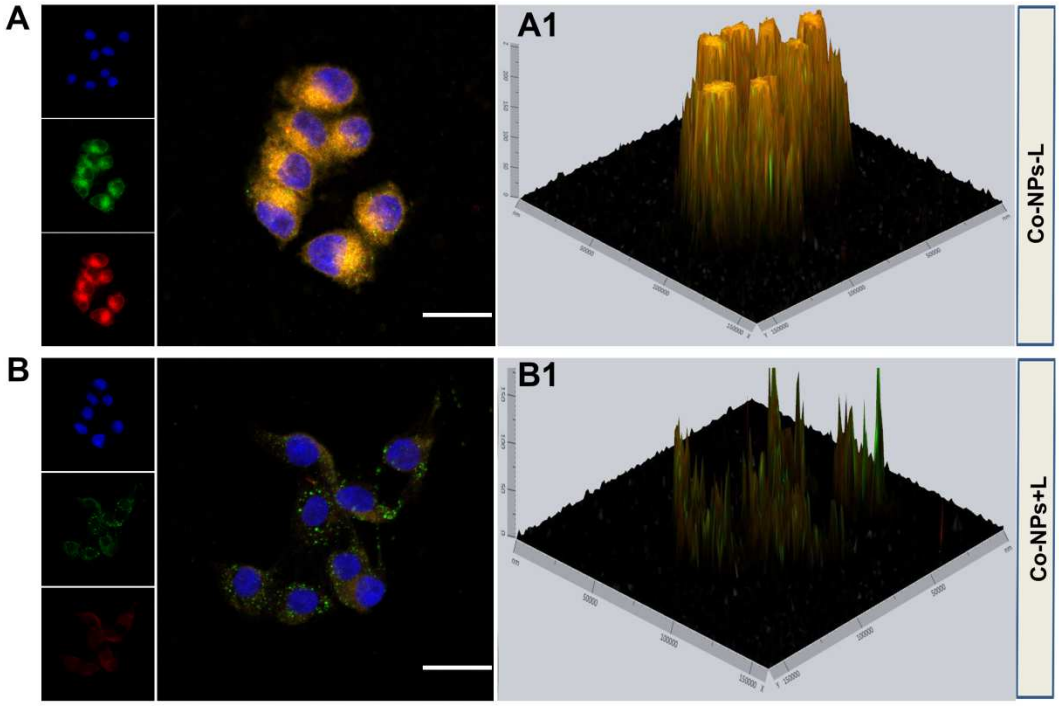

Fig 5. (A-B) Confocal microscopy images of HeLa cells after incubation with Co-NPs without (-L) with (+L) 5 min laser irradiation. (A1-B1) Quantitative analysis of the fluorescence of Co-NPs and Lyso-tracker Red in cells from 2.5D image. For each panel, the images from above to down show cell nuclei stained by DAPI (blue), Co-NPs fluorescence in cells (green), lysosomes stained with Lyso-tracker Red (red) and overlays of three images. Scale bars, 20 μm.

When light irradiation with just 3 min was employed at the initial time of cells incubated with Co-NPs, enhanced cellular uptake was observed. Obviously, the irradiated group emits a brighter fluorescence than the non-irradiated group (Fig S6). The enhanced cell uptake was ascribed to the photochemical internalization (PCI) effect.[51-53] PCI-induced internalization of the Co-NPs was furthered demonstrated by flow cytometric analysis. In Fig 4B and 4B1, the group of Co-NPs in HeLa cells with light irradiation displays the enhanced cellular internalization of the Co-NPs compared with the control. In order to validate the PCI induced internalization result from 2PE-PS, the flow cytometric analyses of NPs (PTX-SS + Nile Red) with or without 3 min light irradiation were also carried out. The significant difference (**$p < 0.01$) in the cellular internalization after light illumination further demonstrate the photochemical internalization process. The results (Fig 4C, C1, Fig S6B) demonstrated that there was no noteworthy difference in the cellular endocytosis, indicating that 2PE-PS play a vital role during the process of PCI-induced

internalization. Moreover, the negligible significant difference result (#p > 0.05) also corroborates that it is the photosensitizer-2PE-PS that induce the PCI process. In addition, lysosomal permeability was investigated by (AO) staining.[54] When AO concentrated in lysosomes, it emits a granular red fluorescence, whereas it would emit a diffuse green fluorescence in cytosol. A reduction in red fluorescence along with an increased green fluorescence in cytosol shows a relocation of AO from the lysosomes to the cytosol, followed by the change of lysosome permeability because of the ROS produced by 2PE-PS (Fig S7).

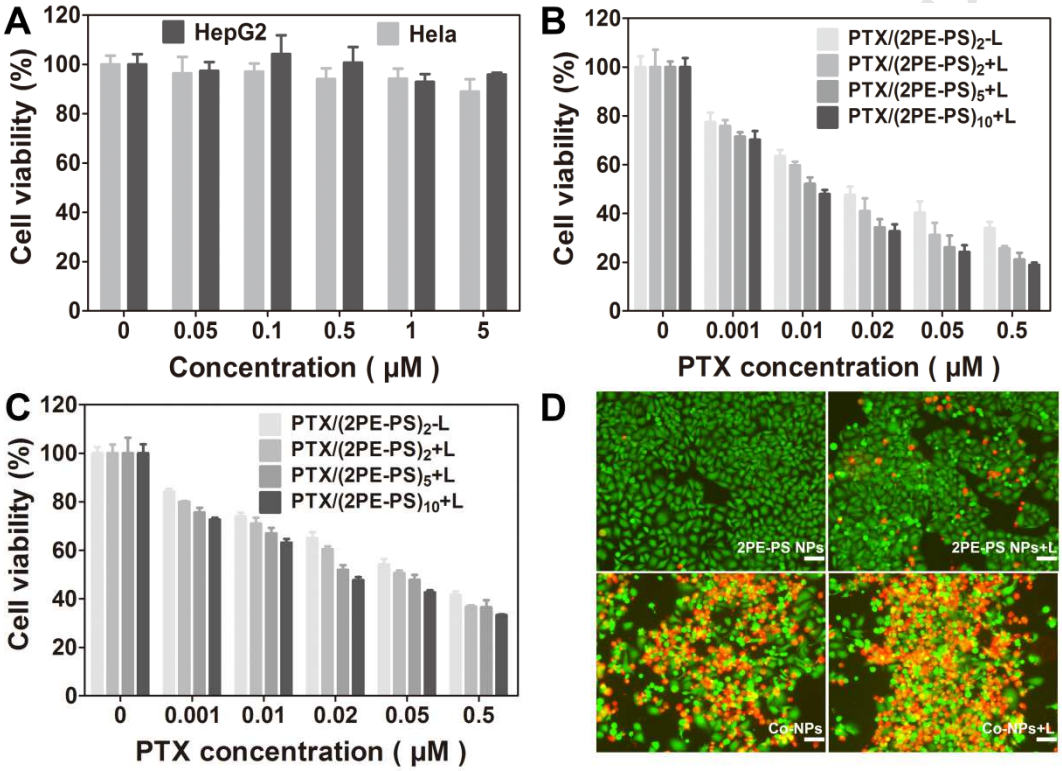

Fig 6. In vitro synergistic therapy efficacy of Co-NPs. (A) Relative cell viabilities of HepG2 and HeLa cells incubated with different concentrations of 2PE-PS NPs. Cell viabilities of HeLa cells (B) and HepG2 cells (C) incubated with different molar ratios of Co-NPs upon an 808 nm laser irradiation at 1 W/cm^2 for 15 min. (D) Fluorescence microscope images of calcein AM (green, live cells) and Propidium Iodide (red, dead cells) co-cultured HeLa cells pretreated with 2PE-PS NPs without or with irradiation, Co-NPs in dark and Co-NPs upon irradiation for 15 min, Scale bars, 40 μm.

Cytotoxicity results

Standard thiazolyblue tetrazolium bromide (MTT) assay was used to evaluate the cytotoxicity of Co-NPs against human hepatocellular carcinoma (HepG2) and HeLa cells. 2PE-PS NPs exhibited a negligible cytotoxicity without irradiation at the concentration of up to 5 μM after 48 h incubation, implying that 2PE-PS NPs have favorable biocompatibility (Fig 6A). Although 2PE-PS shows better anticancer effect under low power 450 nm light irradiation (one photon) contrast to 808 nm laser

irradiation (two photon) (Fig S8), 808 nm light resource was employed because of the depth of tissue penetration in subsequent experiments. Under irradiation with a laser of 808 nm, a dose-dependent cytotoxicity of Co-NPs is observed towards both HepG2 and HeLa cells (Fig 6B-C). Co-NPs with three different molar ratios of PTX to 2PE-PS were designed to explore the synergetic effect of chemotherapy and photodynamic therapy. Compared to Co-NPs in dark, the corresponding half-maximal inhibitory concentration (IC50) against HepG2 and HeLa become lower and lower along with increasing of proportion of 2PE-PS in Co-NPs. The corresponding IC50 values are listed in Table S2. The IC50 value of Co-NPs in dark against HeLa cells is 0.03 μM, while the values of Co-NPs after irradiation under an 808 nm laser are 0.011，0.003，0.0027 μM for PTX/2PE-PS_2, PTX/2PE-PS_5 and PTX/2PE-PS_{10}, respectively. Moreover, the anticancer efficiency of Co-NPs was examined by the live/dead staining (Fig 6D). Almost all of the HeLa cells were dead after being incubated with the Co-NPs under irradiation, which was the synergistic therapeutic effect of chemotherapy of PTX and photodynamic therapy of 2PE-PS. Obviously, the combination therapy offers some advantages over single treatment.

Antitumor activity

To verify the in vivo anticancer efficacy, intratumor injection was employed to deliver Co-NPs into the mice bearing human cervical cancer tumors at the doses of 1.9 mg/kg of PTX/2PE-PS_5 with an 808 nm laser irradiation at 1.5 W/cm^2 for 15 min, followed by the tumor volume and body weight measurements. As shown in Fig 7A-F, PBS injection and laser irradiation as a control displayed a sharp tumor growth. In the absence of irradiation, Co-NPs had a relatively satisfied tumor inhibition effect as compared to that of control group due to the favorable therapeutic effect of paclitaxel (Fig 7B). Upon irradiation, tumors were almost completely clear away (Fig 7C). After 20 days of observation, the tumors were harvested from three groups. The weights and sizes of tumors treated with Co-NPs were significantly smaller than for the control group (Fig 7D, 7F). The obvious significant difference (***$P < 0.001$) in the tumor volume and tumor weight between the control and drug-treated groups well affirmed the tumor inhibition effect of as-prepared Co-NPs. Moreover, the body weights of mice were not significant influenced by various treatments, suggesting that Co-NPs treatment have no obvious system toxicity (Fig 7G).

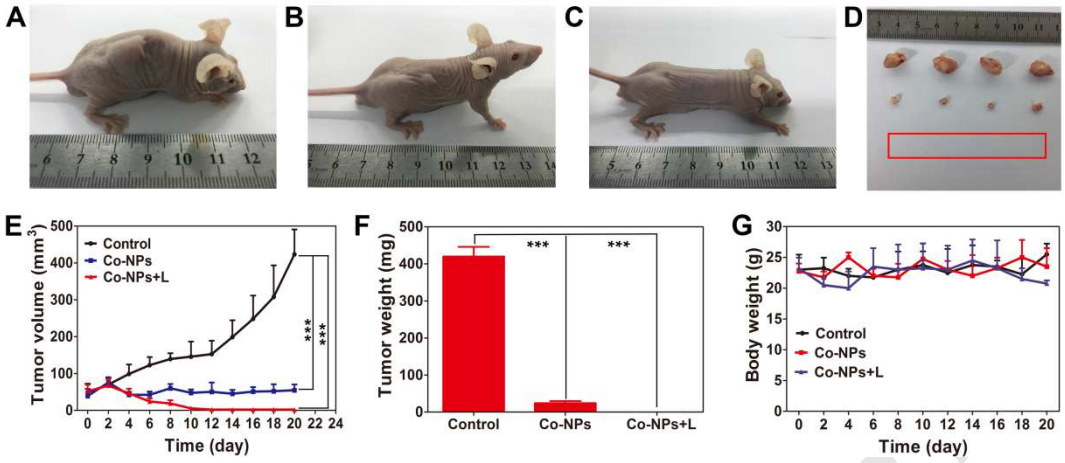

Fig 7. In vivo anticancer efficacy. Various groups treated with (A) PBS+Laser as control, (B) Co-NPs, (C) Co-NPs+Laser. (D) Photo of excised tumor. From top to down: PBS+Laser, Co-NPs and Co-NPs+Laser group. (E) Change of tumor volumes of three groups. (F) Tumor weight of three groups. (G) Body weight of mice after different treatments. Statistical significance: ***P < 0.001.

Conclusion

In conclusion, an organic nanoparticle was constructed to enhance anticancer efficiency by combining chemotherapy and PDT. Due to the similar symmetric structure, PTX dimers and two-photo dyes could assemble into spherical and stable nanoscale Co-NPs. The Co-NPs indicate the enhanced cellular uptake and endosomal escape upon irradiation due to the production of ROS, which result in the synergistic enhancement of cytotoxicity towards cancer cells. These Co-NPs possess effective ability of inhibiting the growth of human cervical cancer tumors upon NIR laser irradiation. This work emphasizes the great potential of using molecular self-assembly to develop state-of-art nanomedicines for cancer therapy.

Acknowledgements

This work was supported by the National Natural Science Foundation of China (Project nos. 81602715) and Postdoctoral Science Foundation of China (Project nos. 2018T110256).

References

[1] Peer D, Karp JM, Hong S, Farokhzad OC, Margalit R, Langer R. Nanocarriers as an emerging platform for cancer therapy. Nat Nanotechnol. 2007;2:751.
[2] Zhang T, Zhang W, Zheng M, Xie Z. Near-infrared BODIPY-paclitaxel conjugates assembling organic nanoparticles for chemotherapy and bioimaging. J Colloid Interface Sci. 2018;514:584-91.
[3] García Calavia P, Chambrier I, Cook MJ, Haines AH, Field RA, Russell DA.

Targeted photodynamic therapy of breast cancer cells using lactose-phthalocyanine functionalized gold nanoparticles. J Colloid Interface Sci. 2018;512:249-59.
[4] Yi X, Yang K, Liang C, Zhong X, Ning P, Song G, et al. Imaging-Guided Combined Photothermal and Radiotherapy to Treat Subcutaneous and Metastatic Tumors Using Iodine-131-Doped Copper Sulfide Nanoparticles. Adv Funct Mater. 2015;25(29):4689-99.
[5] Huang C, Chu C, Wang X, Lin H, Wang J, Zeng Y, et al. Ultra-high loading of sinoporphyrin sodium in ferritin for single-wave motivated photothermal and photodynamic co-therapy. Biomater Sci. 2017;5(8):1512-6.
[6] Li J, Wang X, Zheng D, Lin X, Wei Z, Zhang D, et al. Cancer cell membrane-coated magnetic nanoparticles for MR/NIR fluorescence dual-modal imaging and photodynamic therapy. Biomater Sci. 2018;6(7):1834-45.
[7] Liu L, Wang R, Wang C, Wang J, Chen L, Cheng J. Light-triggered release of drug conjugates for an efficient combination of chemotherapy and photodynamic therapy. Biomater Sci. 2018;6(5):997-1001.
[8] Wang C, Liu L, Cao H, Zhang W. Intracellular GSH-activated galactoside photosensitizers for targeted photodynamic therapy and chemotherapy. Biomater Sci. 2017;5(2):274-84.
[9] Wang D, Niu L, Qiao Z-Y, Cheng D-B, Wang J, Zhong Y, et al. Synthesis of Self-Assembled Porphyrin Nanoparticle Photosensitizers. ACS Nano. 2018;12(4):3796-803.
[10] Yang Z, Sun N, Cheng R, Zhao C, Liu Z, Li X, et al. pH multistage responsive micellar system with charge-switch and PEG layer detachment for co-delivery of paclitaxel and curcumin to synergistically eliminate breast cancer stem cells. Biomaterials. 2017;147:53-67.
[11] Zhang R, Xing R, Jiao T, Ma K, Chen C, Ma G, et al. Carrier-Free, Chemophotodynamic Dual Nanodrugs via Self-Assembly for Synergistic Antitumor Therapy. ACS Appl Mater Interfaces. 2016;8(21):13262-9.
[12] Zhu H, Cheng P, Chen P, Pu K. Recent progress in the development of near-infrared organic photothermal and photodynamic nanotherapeutics. Biomater Sci. 2018;6(4):746-65.
[13] Pei Q, Hu X, Zheng X, Liu S, Li Y, Jing X, et al. Light-Activatable Red Blood Cell Membrane-Camouflaged Dimeric Prodrug Nanoparticles for Synergistic Photodynamic/Chemotherapy. ACS Nano. 2018;12(2):1630-41.
[14] Liu M, Wang L, Zheng X, Liu S, Xie Z. Hypoxia-Triggered Nanoscale Metal–Organic Frameworks for Enhanced Anticancer Activity. ACS Appl Mater Interfaces. 2018;10(29):24638-47.
[15] Xiong H, Zhou D, Zheng X, Qi Y, Wang Y, Jing X, et al. Stable amphiphilic supramolecular self-assembly based on cyclodextrin and carborane for the efficient photodynamic therapy. Chem Commun. 2017;53(24):3422-5.
[16] Lu K, He C, Guo N, Chan C, Ni K, Weichselbaum RR, et al. Chlorin-Based Nanoscale Metal–Organic Framework Systemically Rejects Colorectal Cancers via Synergistic Photodynamic Therapy and Checkpoint Blockade Immunotherapy. J Am Chem Soc. 2016;138(38):12502-10.

[17] Wang X, Lin Y, Li X, Wang D, Di D, Zhao Q, et al. Fluorescent carbon dot gated hollow mesoporous carbon for chemo-photothermal synergistic therapy. J Colloid Interface Sci. 2017;507:410-20.
[18] Ganta S, Devalapally H, Shahiwala A, Amiji M. A review of stimuli-responsive nanocarriers for drug and gene delivery. J Controlled Release. 2008;126(3):187-204.
[19] Qin S-Y, Zhang A-Q, Cheng S-X, Rong L, Zhang X-Z. Drug self-delivery systems for cancer therapy. Biomaterials. 2017;112:234-47.
[20] Huang P, Wang D, Su Y, Huang W, Zhou Y, Cui D, et al. Combination of Small Molecule Prodrug and Nanodrug Delivery: Amphiphilic Drug–Drug Conjugate for Cancer Therapy. J Am Chem Soc. 2014;136(33):11748-56.
[21] Mou Q, Ma Y, Zhu X, Yan D. A small molecule nanodrug consisting of amphiphilic targeting ligand–chemotherapy drug conjugate for targeted cancer therapy. J. Controlled Release. 2016;230:34-44.
[22] Zou Q, Abbas M, Zhao L, Li S, Shen G, Yan X. Biological Photothermal Nanodots Based on Self-Assembly of Peptide–Porphyrin Conjugates for Antitumor Therapy. J Am Chem Soc. 2017;139(5):1921-7.
[23] Wang Y, Liu D, Zheng Q, Zhao Q, Zhang H, Ma Y, et al. Disulfide Bond Bridge Insertion Turns Hydrophobic Anticancer Prodrugs into Self-Assembled Nanomedicines. Nano Letters. 2014;14(10):5577-83.
[24] Zheng X, Li Z, Chen L, Xie Z, Jing X. Self-Assembly of Porphyrin–Paclitaxel Conjugates Into Nanomedicines: Enhanced Cytotoxicity due to Endosomal Escape. Chem. Asian J. 2016;11(12):1780-4.
[25] Li Z, Zheng M, Guan X, Xie Z, Huang Y, Jing X. Unadulterated BODIPY-dimer nanoparticles with high stability and good biocompatibility for cellular imaging. Nanoscale. 2014;6(11):5662-5.
[26] Zhang W, Lin W, Zheng X, He S, Xie Z. Comparing Effects of Redox Sensitivity of Organic Nanoparticles to Photodynamic Activity. Chem Mater. 2017;29(4):1856-63.
[27] Zheng X, Wang L, Liu S, Zhang W, Liu F, Xie Z. Nanoparticles of Chlorin Dimer with Enhanced Absorbance for Photoacoustic Imaging and Phototherapy. Adv Funct Mater. 2018;28(26):1706507.
[28] Pei Q, Hu X, Liu S, Li Y, Xie Z, Jing X. Paclitaxel dimers assembling nanomedicines for treatment of cervix carcinoma. J Controlled Release. 2017;254:23-33.
[29] Miao Q, Pu K. Organic Semiconducting Agents for Deep-Tissue Molecular Imaging: Second Near-Infrared Fluorescence, Self-Luminescence, and Photoacoustics. Adv Mater. 2018;30(49):1801778.
[30] Pei Q, Hu X, Zhou J, Liu S, Xie Z. Glutathione-responsive paclitaxel dimer nanovesicles with high drug content. Biomater Sci. 2017;5(8):1517-21.
[31] Liu LH, Qiu WX, Li B, Zhang C, Sun LF, Wan SS, et al. A Red Light Activatable Multifunctional Prodrug for Image-Guided Photodynamic Therapy and Cascaded Chemotherapy. Adv Funct Mater. 2016;26(34):6257-69.
[32] Wang Y, Wei G, Zhang X, Xu F, Xiong X, Zhou S. A Step-by-Step Multiple Stimuli‐Responsive Nanoplatform for Enhancing Combined Chem-Photodynamic

Therapy. Adv Mater. 2017;29(12):1605357.
[33] Jiang Y, Pu K. Multimodal Biophotonics of Semiconducting Polymer Nanoparticles. Acc Chem Res. 2018;51(8):1840-9.
[34] Li J, Pu K. Development of organic semiconducting materials for deep-tissue optical imaging, phototherapy and photoactivation. Chem Soc Rev. 2019;48(1):38-71.
[35] Li J, Xie C, Huang J, Jiang Y, Miao Q, Pu K. Semiconducting Polymer Nanoenzymes with Photothermic Activity for Enhanced Cancer Therapy. Angew Chem Int Ed 2018;57(15):3995-8.
[36] Zhen X, Zhang J, Huang J, Xie C, Miao Q, Pu K. Macrotheranostic Probe with Disease-Activated Near-Infrared Fluorescence, Photoacoustic, and Photothermal Signals for Imaging-Guided Therapy. Angew Chem Int Ed 2018;130(26):7930-4.
[37] Gu B, Wu W, Xu G, Feng G, Yin F, Chong Peter Han J, et al. Precise Two-Photon Photodynamic Therapy using an Efficient Photosensitizer with Aggregation-Induced Emission Characteristics. Adv Mater. 2017;29(28):1701076.
[38] Liu H, Yang Y, Wang A, Han M, Cui W, Li J. Hyperbranched Polyglycerol-Doped Mesoporous Silica Nanoparticles for One- and Two-Photon Activated Photodynamic Therapy. Adv Funct Mater. 2016;26(15):2561-70.
[39] Zou Q, Zhao H, Zhao Y, Fang Y, Chen D, Ren J, et al. Effective Two-Photon Excited Photodynamic Therapy of Xenograft Tumors Sensitized by Water-Soluble Bis(arylidene)cycloalkanone Photosensitizers. J Med Chem. 2015;58(20):7949-58.
[40] Zou Q, Zhao Y, Makarov NS, Campo J, Yuan H, Fang D-C, et al. Effect of alicyclic ring size on the photophysical and photochemical properties of bis(arylidene)cycloalkanone compounds. Phys Chem Chem Phys. 2012;14(33):11743-52.
[41] Zheng X, Wang L, Liu M, Lei P, Liu F, Xie Z. Nanoscale Mixed-Component Metal–Organic Frameworks with Photosensitizer Spatial-Arrangement-Dependent Photochemistry for Multimodal-Imaging-Guided Photothermal Therapy. Chem Mater. 2018;30(19):6867-76.
[42] Yang T, Liu L, Deng Y, Guo Z, Zhang G, Ge Z, et al. Ultrastable Near-Infrared Conjugated-Polymer Nanoparticles for Dually Photoactive Tumor Inhibition. Adv Mater. 2017;29(31):1700487.
[43] Yuan Y, Zhang CJ, Liu B. A Photoactivatable AIE Polymer for Light-Controlled Gene Delivery: Concurrent Endo/Lysosomal Escape and DNA Unpacking. Angew Chem Int Ed. 2015;54(39):11419-23.
[44] Zhang P, Li S, Chen H, Wang X, Liu L, Lv F, et al. Biofilm Inhibition and Elimination Regulated by Cationic Conjugated Polymers. ACS Appl Mater Interfaces. 2017;9(20):16933-8.
[45] Zheng X, Wang L, Pei Q, He S, Liu S, Xie Z. Metal–Organic Framework@Porous Organic Polymer Nanocomposite for Photodynamic Therapy. Chem Mater. 2017;29(5):2374-81.
[46] Chen J, Ouyang J, Chen Q, Deng C, Meng F, Zhang J, et al. EGFR and CD44 Dual-Targeted Multifunctional Hyaluronic Acid Nanogels Boost Protein Delivery to Ovarian and Breast Cancers In Vitro and In Vivo. ACS Appl Mater Interfaces. 2017;9(28):24140-7.

[47] Feng L, Cheng L, Dong Z, Tao D, Barnhart TE, Cai W, et al. Theranostic Liposomes with Hypoxia-Activated Prodrug to Effectively Destruct Hypoxic Tumors Post-Photodynamic Therapy. ACS Nano. 2017;11(1):927-37.
[48] Feng L, Gao M, Tao D, Chen Q, Wang H, Dong Z, et al. Cisplatin-Prodrug-Constructed Liposomes as a Versatile Theranostic Nanoplatform for Bimodal Imaging Guided Combination Cancer Therapy. Adv Funct Mater. 2016;26(13):2207-17.
[49] Ye Z, Xiong C, Pan J, Su D, Zeng L. Highly photostable, lysosome-targeted BODIPYs with green to near-infrared emission for lysosome imaging in living cells. Dyes Pigm. 2018;155:30-5.
[50] Zhang C, Liu T, Su Y, Luo S, Zhu Y, Tan X, et al. A near-infrared fluorescent heptamethine indocyanine dye with preferential tumor accumulation for in vivo imaging. Biomaterials. 2010;31(25):6612-7.
[51] Nomoto T, Nishiyama N. Design of drug delivery systems for physical energy-induced chemical surgery. Biomaterials. 2018.
[52] Norum O-J, Fremstedal ASV, Weyergang A, Golab J, Berg K. Photochemical delivery of bleomycin induces T-cell activation of importance for curative effect and systemic anti-tumor immunity. J Controlled Release. 2017;268:120-7.
[53] Shin D, Christie C, Ju D, Nair RK, Molina S, Berg K, et al. Photochemical internalization enhanced macrophage delivered chemotherapy. Photodiagn Photodyn Ther. 2018;21:156-62.
[54] Wang F, Li X, Li W, Bai H, Gao Y, Ma J, et al. Dextran coated Fe3O4 nanoparticles as a near-infrared laser-driven photothermal agent for efficient ablation of cancer cells in vitro and in vivo. Mater Sci Eng: C. 2018;90:46-56.

Graphical abstract

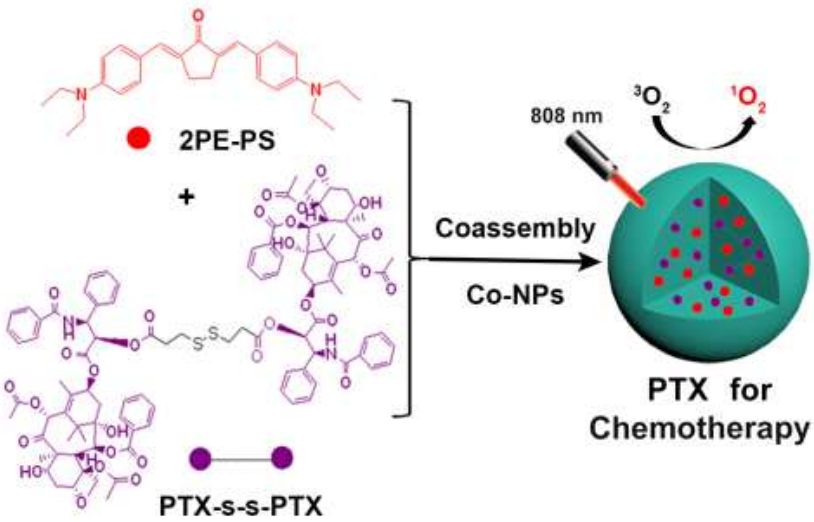

Research highlights

► The first study to apply nanoparticles coassembled by paclitaxel dimer and two-photo photosensitizer.

► The nanoparticles indicates the enhanced cellular uptake and endosomal escape upon irradiation due to the production of ROS

► The nanoparticles possesses synergistic enhancement of cytotoxicity towards cancer cells and growth inhibition of human cervical cancer tumors